Multiple octupole-type band structures in ^{220}Th: Reflection-asymmetric tidal waves?

W. Reviol,[1] C. J. Chiara,[1] M. Montero,[1] D. G. Sarantites,[1] O. L. Pechenaya,[2] M. P. Carpenter,[3] R. V. F. Janssens,[3] T. L. Khoo,[3] T. Lauritsen,[3] C. J. Lister,[3] D. Seweryniak,[3] S. Zhu,[3] and S. G. Frauendorf[4]

[1]*Department of Chemistry, Washington University, St. Louis, Missouri 63130, USA*
[2]*Department of Physics, Washington University, St. Louis, Missouri 63130, USA*
[3]*Physics Division, Argonne National Laboratory, Argonne, Illinois 60439, USA*
[4]*Department of Physics, University of Notre Dame, Notre Dame, Indiana 46556, USA*

(Received 23 August 2006; published 12 October 2006)

The ^{220}Th level scheme has been considerably extended from an experiment using the ^{26}Mg + ^{198}Pt reaction at 128 MeV. The evaporation residues from this very fissile system were selected with the HERCULES detector system and residue-gated γ rays were measured with Gammasphere. The simplex feature (alternating-parity levels) persists up to the highest spins observed ($23\hbar$), but the nucleus exhibits a more vibrational-like behavior than the heavier Th isotopes. In addition, a doubling of the negative-parity, odd-spin states is seen as well as a staggering of the $B(E1)/B(E2)$ ratios. A new interpretation based on a picture of tidal waves on a reflection-asymmetric nuclear surface is proposed.

DOI: 10.1103/PhysRevC.74.044305 PACS number(s): 27.90.+b, 23.20.Lv, 23.20.En, 21.60.−n

I. INTRODUCTION

In the actinide region, octupole correlations have a large impact on nuclear structure at low excitation energy [1,2]. Experimentally, a characteristic signature for octupole correlations is the appearance of alternating-parity level sequences connected by strong electric dipole transitions. Two distinct modes of octupole collectivity have been established so far. In nuclei around ^{224}Th, evidence for the rotational mode is found, implying a nuclear shape with stable octupole and quadrupole deformation. Here, the members of the ground-state sequence with spin and parity $(I+1)^+$ decay to I^- levels that, in turn, decay to $(I-1)^+$ levels. In nuclei around ^{236}U, on the other hand, bandlike sequences built on octupole surface vibrations are observed. The lower-spin members of these bands are involved in decays from I^- to both $(I-1)^+$ and $(I+1)^+$ levels; here the positive-parity levels are always yrast. However, the two modes of octupole collectivity are also related to each other in that a transition from an octupole vibration to stable octupole deformation may occur as the spin or proton number increases. Such a change seems to be supported by recent data for $^{238-240}$Pu [3,4].

Departing from the center of stable octupole deformation around ^{224}Th (neutron number $N = 134$) toward the lighter isotopes, another transitional region is traversed. At the lighter end of this region, near $N = 126$, a spherical nuclear shape governs the yrast structure, and noncollective excitations characterize the yrast line. In a study of the $N = 130$ nucleus ^{218}Ra, Schulz *et al.* [5] suggested that some nuclei may assume a shape with a considerable octupole deformation but a negligible quadrupole deformation. To learn about this behavior in detail and possibly establish a new type of octupole collectivity, a study of the heavier isotone ^{220}Th is a natural next step.

Rather little is known about excited states in ^{220}Th due to the low production of the nucleus in a fusion-evaporation reaction where fission is a strong competing channel. The ground-state decay was first reported by Häusser *et al.* [6]. The in-beam study of ^{220}Th by Bonin *et al.* [7] and an unpublished thesis [8] led to the observation of an alternating-parity or simplex-partner band [9], which provided first evidence of octupole collectivity in this nucleus. In this work, levels with spin and parity up to $I^\pi = 10^+$ (tentatively 14^+) and $I^\pi = 15^-$ (tentatively 19^-) were reported. The published level structure of ^{220}Th was also summarized in Fig. 13 of Ref. [1].

As discussed in, e.g., Ref. [7], detailed spectroscopic studies of light Th nuclei, such as ^{220}Th, require that a "filter" device be used to separate the γ rays emitted by the evaporation residues from those of the dominant fission products. For this purpose, Bonin *et al.* [7] used an electrostatic separator. It is desirable to choose a very asymmetric reaction, which leads, through the $\pi\lambda\!\!\!^{-2}$ factor [10], to a larger residue cross section and to less fission than is the case with a more symmetric channel. For the present study of ^{220}Th, the ^{26}Mg + ^{198}Pt $\rightarrow$ ^{224}Th* reaction was used in conjunction with a setup combining Gammasphere [11] and the 64-element evaporation-residue detector HERCULES [12]. The latter device is particularly suitable for very asymmetric reactions and targets with thicknesses in excess of 0.5 mg/cm^2.

The present article reports results for the main channel in the reaction, 4 n evaporation, leading to ^{220}Th. A new level scheme for ^{220}Th is presented, with the simplex-partner band firmly established up to $I^\pi = 20^+$ and $I^\pi = 21^-$. Several nonyrast level structures were delineated as well. The analogy with the level scheme of ^{218}Ra is discussed as is a notable difference: only ^{220}Th possesses two negative-parity, odd-spin sequences. Special attention is focused on the measured $B(E1)/B(E2)$ ratios, including their staggering between even and odd spins.

II. EXPERIMENTAL CONDITIONS

The experiment was performed at the ATLAS accelerator at Argonne National Laboratory. A 128-MeV ^{26}Mg beam was focused on a 0.88-mg/cm^2 Pt target enriched to 92% in

mass 198. The beam intensity varied between 2 and 3 pnA over the duration of the experiment. Gammasphere comprised 98 HPGe detectors with BGO Compton-suppression shields, arranged in 15 rings of constant angle around the target. Five of the HPGe detectors did not have the hevimet collimators installed because of geometrical constraints. Absorbers in front of each HPGe detector, consisting of 0.05-mm Ta and 0.25-mm Cu, absorbed most of the unwanted target x rays. The detection efficiency of Gammasphere for low-energy γ rays was optimized by operating the timing discriminators in leading-edge rather than in constant-fraction mode. The front of the HERCULES detectors was located 24 cm from the target and the device subtended polar angles from 6.1° to 25.5° with respect to the beam axis. Two parameters were measured with HERCULES: the time-of-flight (ToF) of reaction products and scattered beam and the pulse height (PH) of the signal from each detector hit by a particle. The event trigger required a minimum of three Compton-suppressed γ rays in prompt coincidence. The information from any of the HERCULES detectors that was correlated with the event trigger was accepted as well.

III. ANALYSIS AND RESULTS

The γ rays from evaporation-residue nuclei were selected by two-dimensional gating on the parameters ToF and PH. The energies of these γ rays were corrected for the Doppler shifts by using the observed residue direction. The γ-ray energies of coincident transitions were then sorted into an E_γ-E_γ matrix, an E_γ-E_γ-E_γ cube, and a set of E_γ-E_γ matrices for different Gammasphere rings (to determine γ-ray angular distributions). Sample γ-ray spectra are presented in Fig. 1.

In the "raw" γ-ray spectrum of Fig. 1(a), the peaks of interest, such as the 233.9-keV transition in ^{220}Th, are barely visible above background. The impact of residue gating is demonstrated by the total projection of Fig. 1(b), where the peak-to-background ratio has improved by two orders of magnitude. In the present reaction, the residue detection efficiency is measured to be 59(4)%. This number is based on a comparison between residue-γ-γ and "raw" γ-γ coincidence data; i.e., on the γ-ray intensity ratio measured for the strongest peaks in spectra derived from the two matrices by gating on a prominent transition in ^{220}Th. A "raw" total projection spectrum, like in Fig. 1(a), does not allow an accurate measurement of peak intensities, because of the large background due to fission and the resulting poor peak-to-total for all γ rays.

The spectrum of Fig. 1(b) shows that, in the ^{26}Mg + ^{198}Pt reaction, the *xn* and αxn channels compete in intensity, whereas the *pxn* channels are negligible. Among the αxn channels, the $\alpha 3n$ one leading to ^{217}Ra [13] is most intense. There is no clear evidence for the population of the 3 *n* channel that would lead to ^{221}Th. However, the spectrum of Fig. 1(b) contains γ rays of considerable strength (E_γ = 513, 564 keV) that can be assigned to ^{219}Th [14]. For this nucleus, no excited states had been reported thus far. A ^{219}Th level scheme will be presented in a forthcoming publication [15].

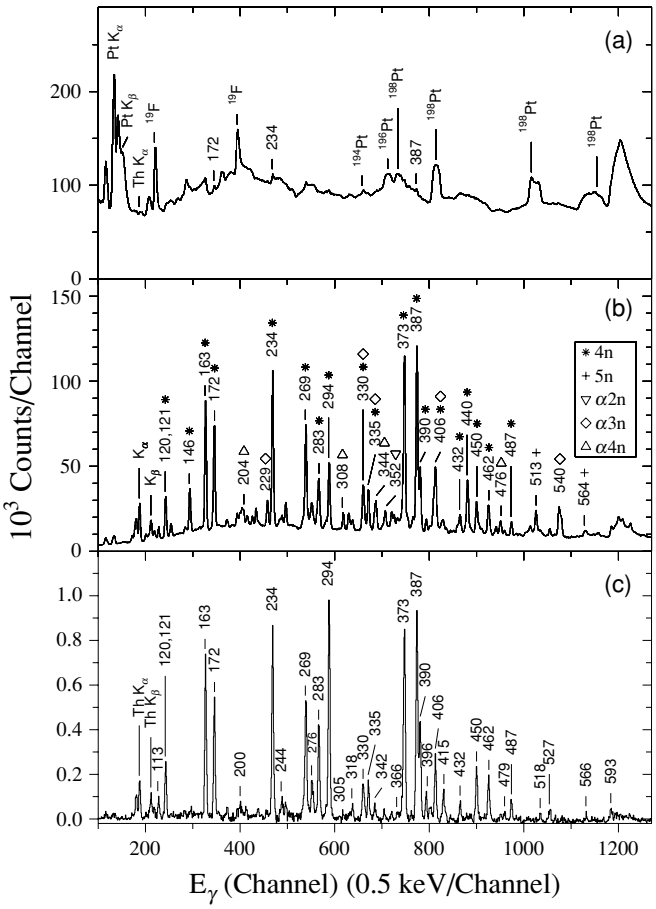

FIG. 1. Sample γ-ray spectra for the 128-MeV ^{26}Mg + ^{198}Pt reaction. (a) The "raw" spectrum with a Doppler-shift correction applied (recoils are assumed to travel along the beam axis). A fraction of the data is shown. (b) The projection of a coincidence matrix for residue-gated γ rays (Doppler-shift correction based on the residue direction). Transitions are labeled by their energies in keV with a symbol for the evaporation channel as defined in the figure. The composite K x-ray peaks are also visible. (c) A coincidence spectrum for ^{220}Th obtained by gating on the 146.1-keV transition.

The spectrum of Fig. 1(c) is a sample residue- and γ-gated spectrum for ^{220}Th where the gating transition (E_γ = 146.1 keV) is the highest-lying dipole transition in the level scheme of Refs. [1,7] ($11^- \rightarrow 10^+$). Figures 2 and 3 provide sets of γ-ray coincidence spectra for ^{220} Th, each gated by an even weaker transition. These spectra are representative for the level sequences in ^{220}Th discussed in Sec. IV.

For most of the γ rays in ^{220}Th, a seven-point angular distribution W(θ) has been measured. Gates on transitions in ^{220}Th are applied with the gating γ ray taken for any Gammasphere detector that had fired. The W (θ) values are determined for groups of adjacent Gammasphere rings with the following angles (obtained from averaged $\cos^2\theta$ values) with respect to the beam axis: θ = 37.4°, 52.8°, 69.8°, 82.8°, 110.2°, 127.2°, and 153.1°. Using a standard Legendre polynomial fit, A_2/A_0 coefficients are derived for $A_4 = 0$ (best fit). Table I lists these coefficients, together with the corresponding spin and parity assignments, level energies,

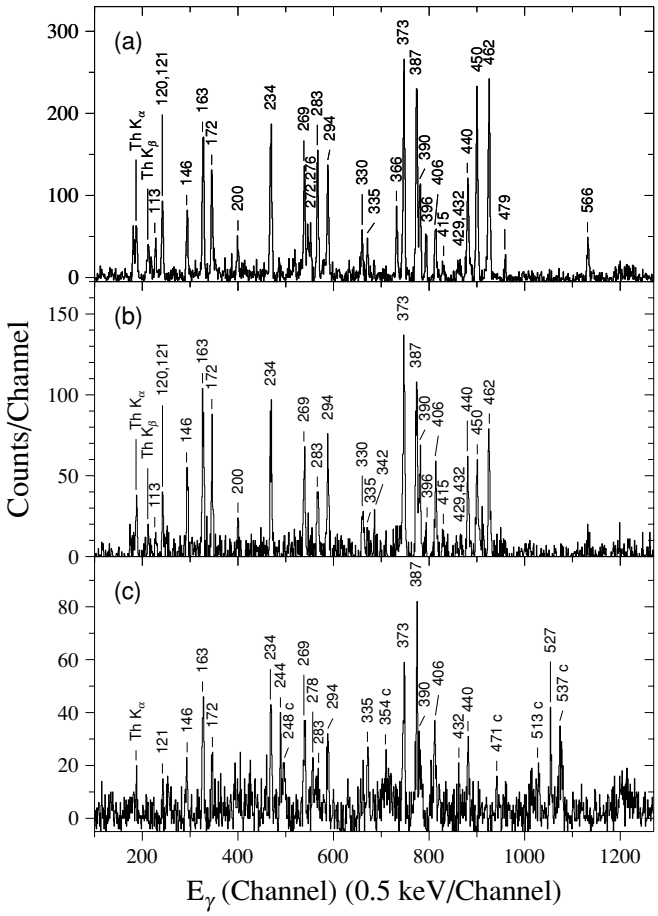

FIG. 2. Representative γ-ray coincidence spectra for the sequences observed in ^{220}Th. (a) The spectrum gated by the 486.5-keV transition. (b) The spectrum gated by the 399.9-keV transition. (c) The spectrum gated by the 517.5-keV transition. Contaminant γ rays, labeled c are from ^{219}Th.

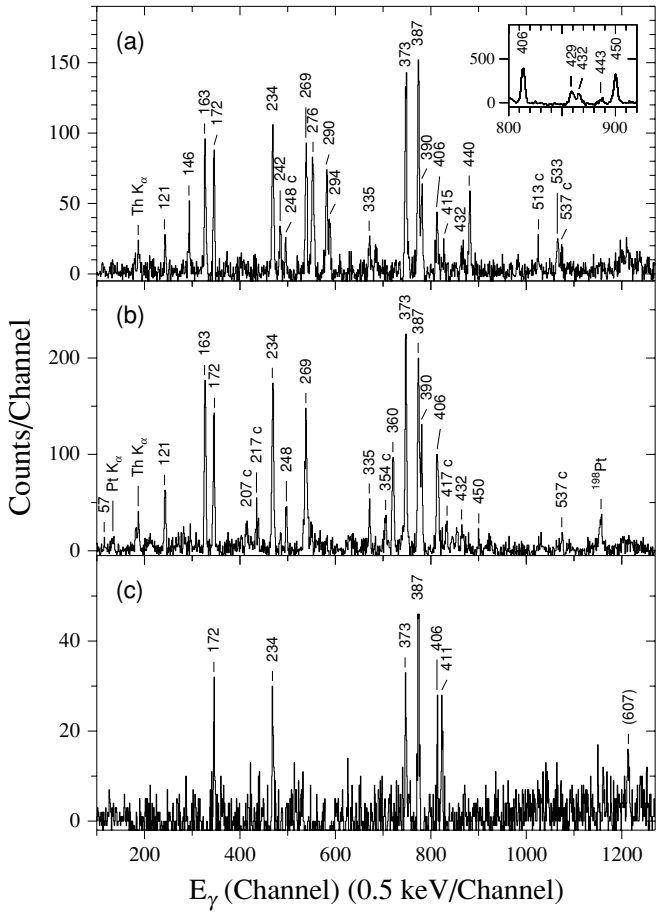

FIG. 3. Similar to Fig. 2, but for gating transitions with the respective energies (a) 592.7 keV, (b) 382.7 keV, and (c) 768 keV. The inset of panel (a) shows a part of the coincidence spectrum gated by the 293.8-keV transition (see text). The spectrum in panel (b) is contaminated by γ rays from ^{198}Pt target recoils.

γ-ray energies, and intensities; the table is organized according to the individual sequences in the level scheme.

IV. LEVEL SCHEME OF ^{220}Th

The level scheme for ^{220}Th is presented in Fig. 4, with the yrast states observed up to $I^\pi = (23^-)$ and $E = 4892$ keV. For almost all transitions, γ-ray angular distributions have been measured and multipolarities have been assigned considering only stretched electric quadrupole ($E2$) transitions and dipole radiation of both electric ($E1$) and magnetic ($M1$) character. Except for the (22^+) and (23^-) levels and three off-yrast states, all spins were firmly established. For the low-lying dipole transitions reaching states with final spins at and below $I^\pi = 7^-$ and 8^+, the parity assignments are supported further by arguments based on the balance between feeding and decay intensity (corrected for internal conversion). These transitions must be of $E1$ character, as the $E1$ conversion coefficients are significantly smaller than the $M1$ coefficients. Otherwise, the feeding intensity of the 0^+ and the 2^+ state would be a factor of 2 weaker than the intensity obtained for the states located directly above ($I \leqslant 8$). The assignments for the higher-lying, negative-parity states follow in many cases from the $E2$ transitions involved.

The yrast band: The states above 10^+ in the positive-parity, ground-state sequence and the states above 11^- in the negative-parity sequence labeled (a) do either extend the ^{220}Th level scheme of Refs. [1,7] or are rearranged as compared to the latter. Specifically, the 396.4-keV $13^-_1 \rightarrow 11^-$ transition was not placed in the previous level scheme. Hence, the spin assignments for the 449.7 and 462.4-keV γ rays proposed here differ from those of the previous level scheme. It is obvious that, just above the 11^- state, sequence (a) shows an irregularity in an $I(\hbar\omega)$ plot ($\hbar\omega \simeq \mathrm{E}_\gamma/2$), reminiscent of a backbending. A representative spectrum for this sequence and related states is shown in Fig. 2(a).

Above the 7^- state, and up to the highest spins observed, sequence (a) remains yrast. This structure, together with the positive-parity ground-state sequence, forms a simplex-partner band, introduced in Sec. I. However, unlike in the heavier even-mass Th nuclei (cf. Fig. 13 of Ref. [1]), there is a distinct staggering of the $E1$ transition energies between transitions originating from states with even and odd spins in ^{220}Th. In fact, with increasing spin, sequence (a) becomes energetically

favored and the staggering becomes more pronounced as a result. Accordingly, the $(I+1)^+ \rightarrow I^-$ transitions compete favorably for strength with the $(I+1)^+ \rightarrow (I-1)^+ E2$ transitions; i.e., the positive-parity, high-spin levels are established by their decay-out dipole transitions rather than by their $E2$ transitions. Nevertheless, both simplex-partners are present up to the highest spins observed. A coincidence spectrum for a high-spin dipole transition is given in Fig. 2(b).

The negative-parity yrare sequences: A second negative-parity, odd-spin sequence, labeled (b) in Fig. 4, is established by the 527.3-keV $13_2^- \rightarrow 11^- E2$ transition. Figure 2(c) is a representative spectrum for this level structure. Perhaps most significant in this spectrum is the absence of the otherwise prominent 449.7 and 462.4-keV transitions. The problem with extending this structure toward higher spins is that the positive-parity sequence, to which structure (b) decays, becomes relatively weak as the spin increases. This reflects, once more, the fact that the spectrum is dominated by the yrast transitions of sequence (a). The $17_2^{(-)}$ level ($E =$ 3681 keV) is tentatively assigned, as this level decays through a weak 305.1-keV transition that is coincident with the 449.7-keV line and the γ rays from states below (including the 371.6/373.3-keV doublet). No 19_2^- state could be established. A candidate transition from this state to lower-lying levels is the 342-keV γ ray seen in Fig. 2(b). However, this 342-keV γ ray has not been placed in the level scheme due to complications introduced by the prominent 343.5/344.2-keV doublet in ^{216}Ra ($\alpha 4n$ channel, cf. Fig. 1(b) and Ref. [13]). At the highest spins, a 21_2^- state ($E = 4520$ keV) is established by the 566.2-keV $E2$ transition, and it is reasonable to assume that this state is a member of sequence (b). The important observation is that there is a *doubling* of negative-parity, odd-spin states in ^{220}Th.

There is also evidence for a short sequence of negative-parity states with even spins labeled (c) in Fig. 4. Figure 3(a) is a representative spectrum for this structure. The 275.6-keV transition is assigned as being of $M1$ character, based on the following arguments. The states of sequence (c) do not decay according to the pattern of dipole and crossover $E2$ transitions, which the ground-state sequence and sequences (a) and (b) have in common. This difference is perhaps most evident from the coincidence relationships of the 293.8-keV transition; the range in the coincidence spectrum around the 429.3-keV $12^+ \rightarrow 10^+$ transition is important [see inset of Fig. 3(a)]. If the 275.6-keV γ ray would be an $E1$ transition, as the by-passing 282.8-keV transition is, the spectrum would also show a transition of about 422 keV (275.6 keV + 146.1 keV) and of similar strength as the 429.3-keV transition. However, such a 422-keV γ ray is absent. The second argument is related to the intensity balance for the 13_1^- state. The 275.6-keV transition is in coincidence with the transitions above this state. For the 121-keV connecting transition, a member of a triplet, an intensity value $I_\gamma \leqslant 1.9$ is reported in Table I. This transition must be of the $M1$ type (implying a conversion coefficient $\alpha_{tot} = 11.48$), to keep feeding and decay intensities in balance. Consequently, the 275.6-keV transition is also a $M1$ transition. The sequence (c) has similarities with the side band in the ^{218}Ra isotone [5],

TABLE I. The γ-ray transitions in ^{220}Th.

I_i^π [a]	E (keV) [b]	E_γ (keV)	I_γ [c]	A_2/A_0 [d]
		Ground-state sequence		
2^+	373	373.3(1)	100	0.085(3)
4^+	760	386.5(1)	94.5(12)	0.200(2)
6^+	1166	406.3(1)	26.7(7)	0.323(46)
6^+	1166	172.2(1)	39.1(4)	−0.187(9)
8^+	1599	432.4(2)	8.7(3)	0.200(14)
8^+	1599	269.1(1)	49.6(10)	−0.201(8)
10^+	2014	414.6(2)	4.1(3)	0.219(45)
10^+	2014	293.8(1)	29.7(7)	−0.234(60)
12^+	2443	429.3(3)	3.3(4)	—
12^+	2443	282.8(2)	20.4(8)	−0.40(12)
14^+	2886	442.8(3)	3.5(4)	0.69(45)
14^+	2886	329.7(2)	10.7(6)	−0.33(11)
14^+	2886	199.2(4)	2.9(2)	−0.54(22)
16^+	3378	491.7(4)	0.8(1)	—
16^+	3378	371.6(4)	4.1(2)	−0.42(20)
16^+	3378	173.5(4)	—	—
18^+	3868	399.9(4)	1.7(2)	−0.54(27)
20^+	4320	452.0(5)	1.0(1)	—
20^+	4320	365.9(3)	1.4(2)	−0.213(99)
(22^+)	4716	283(1)	—	—
		Sequence (a)		
5^-	994	233.9(1)	66.5(13)	−0.218(73)
7^-	1329	335.2(2)	15.6(9)	0.199(55)
7^-	1329	162.9(1)	49.1(11)	−0.197(15)
9^-	1719	389.9(2)	29.9(7)	0.220(7)
9^-	1719	120.7(2)	18.3(5)	−0.299(94)
11^-	2159	440.1(2)	26.4(9)	0.183(87)
11^-	2159	146.1(1)	13.9(7)	−0.201(6)
11^-	2159	57.3(4)	∼3	—
13^-	2556	396.4(3)	5.7(3)	0.187(99)
13^-	2556	113.3(2)	5.5(3)	−0.24(13)
13^-	2556	121(1)	$\leqslant 1.9$ [e]	—
15^-	3005	449.7(2)	13.1(5)	0.38(12)
15^-	3005	119.6(3)	1.7(3)	—
17^-	3468	462.4(3)	11.7(6)	0.28(10)
17^-	3468	91.0(3)	—	—
19^-	3954	486.5(3)	6.5(5)	0.316(37)
21^-	4433	479.3(3)	1.2(2)	0.24(12)
(23^-)	4892	458.9(5)	0.8(1)	—
		Sequence (b)		
13^-	2685	527.3(3)	4.0(3)	0.34(13)
13^-	2685	243.6(3)	4.3(4)	−0.205(58)
15^-	3202	517.5(4)	1.7(2)	0.66(19)
15^-	3202	317.8(3)	3.3(3)	—
$17^{(-)}$	3681	305.1(3)	1.0(1)	−0.40(29)
21^-	4520	566.2(4)	1.3(2)	0.37(17)
21^-	4520	199.6(4)	0.5(2)	—
		Other		
—	3480	277.6(3)	1.1(3)	—
20	4226	271.9(3)	1.4(2)	−0.45(15)
—	—	342.1(4) [f]	2.6(2)	−0.149(90)
		Sequence (c), level (c1)		
12^-	2433	275.6(3)	10.7(5)	−0.38(10)
14^-	3026	592.7(4)	3.1(9)	0.45(10)
16^-	3558	532.5(5)	1.0(1)	—

TABLE I. *(Continued.)*

I_i^{π} [a]	E (keV)[b]	E_γ (keV)	I_γ [c]	A_2/A_0 [d]
16^-	3558	241.7(3)	0.5(2)	—
15	3316	289.9(3)	1.4(4)	−0.34(26)
		Sequence (d)		
$10^{(+)}$	2102	382.7(3)	6.7(4)	−0.309(92)
11	2461	359.9(3)	3.2(2)	−0.097(6)
12	2709	248.2(4)	⩽3.8[g]	−0.43(23)
—	2957	248(1)	—	—
		Sequence (e)		
8^+	1934	768(1)	1.9(1)	0.41(15)
8^+	1934	605(1)	∼1	—
10	2345	411.3(4)	1.0(1)	—

[a]Spin and parity of the depopulated state.
[b]Energy of the depopulated state.
[c]Relative γ-ray intensity of the transition normalized to 100 for the 373.3-keV ground-state transition.
[d]Best fit value obtained for $A_4 = 0$.
[e]Upper limit value from a 389.9-keV and 449.7-keV double-gated spectrum.
[f]Unplaced transition.
[g]Upper limit value due to an unresolved doublet.

including the onset of an additional, interlinked structure labeled (c1) in Fig. 4.

The $I = 20$ level at 4226 keV is not viewed as a member of structure (c) nor as a member of the other structures. The presence of another dipole transition ($E_\gamma = 271.9$ keV) at high spin may indicate that the quadrupole collectivity in this nucleus is quite weak.

The off-yrast states: The remaining states are considered as off-yrast and are grouped in Fig. 4 as structures (d) and (e). These sets of states are "independent" structures in the sense that they are not interlinked with each other nor with sequence (c). For example, there is no transition from the $10_2^{(+)}$ ($E = 2102$ keV) level to the 8_2^+ ($E = 1934$ keV) state. Sample coincidence spectra for structures (d) and (e) are given in Figs. 3(b) and 3(c). As a final note, we stress that the presence of a second positive-parity, even-spin structure is inconclusive. The candidate members of such a structure are the aforementioned 8_2^+ and $10_2^{(+)}$ states and the $E = 3480$ keV level feeding sequence (b); the latter may be qualified as off-yrast as well.

Figure 5(a) introduces the $B(E1)/B(E2)$ ratios determined from the γ-ray intensities as a function of the initial spin for the yrast and yrare transitions in ^{220}Th. The large $B(E1)/B(E2)$ ratio obtained for the 13_1^- (yrast) state may be attributed to the loss of $E2$ strength at the backbending. By comparison, the $B(E1)/B(E2)$ ratio for the 13_2^- (yrare) state is considerably smaller. The rather small $B(E1)/B(E2)$ ratio for $I^\pi = 14^+$ is attributed to the spread of $E1$ strength due to the presence of two 13^- final states.

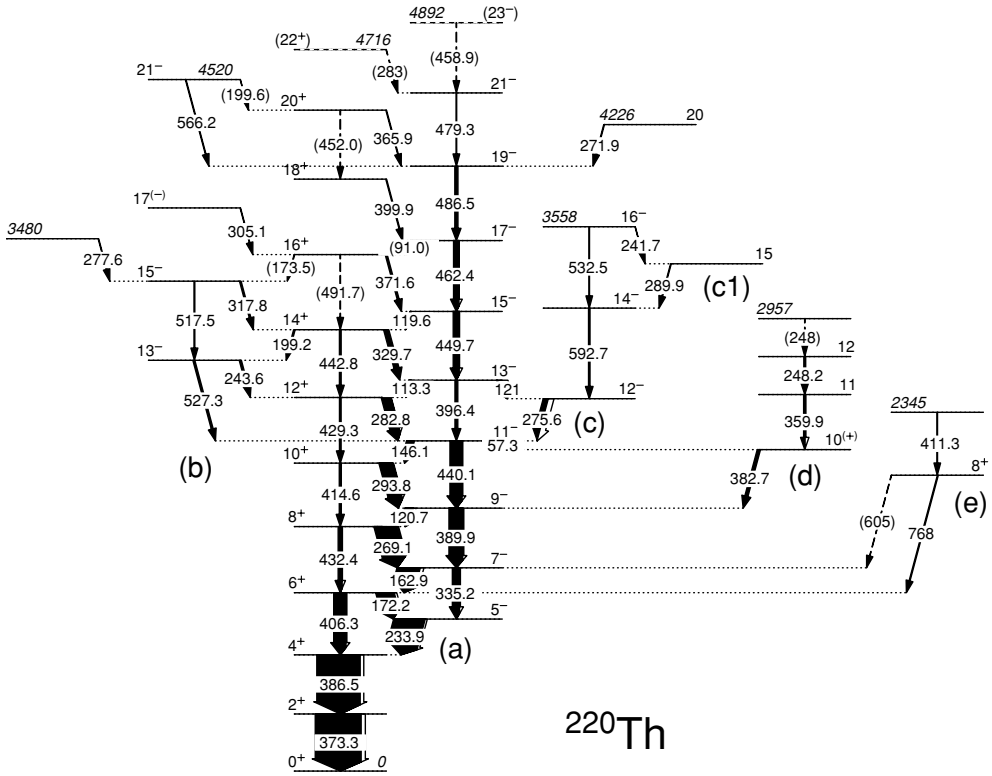

FIG. 4. Proposed level scheme for ^{220}Th. The level spins and parities are given in the figure. The highest-lying state in each sequence and the ground state are also labeled by their energy, in italics. Transitions indicated as dashed arrows, and spins and parities given in parentheses, are considered to be tentative. The energy unit is keV. The widths of the filled and open parts of the arrows are proportional to the γ-ray and internal conversion intensities, respectively.

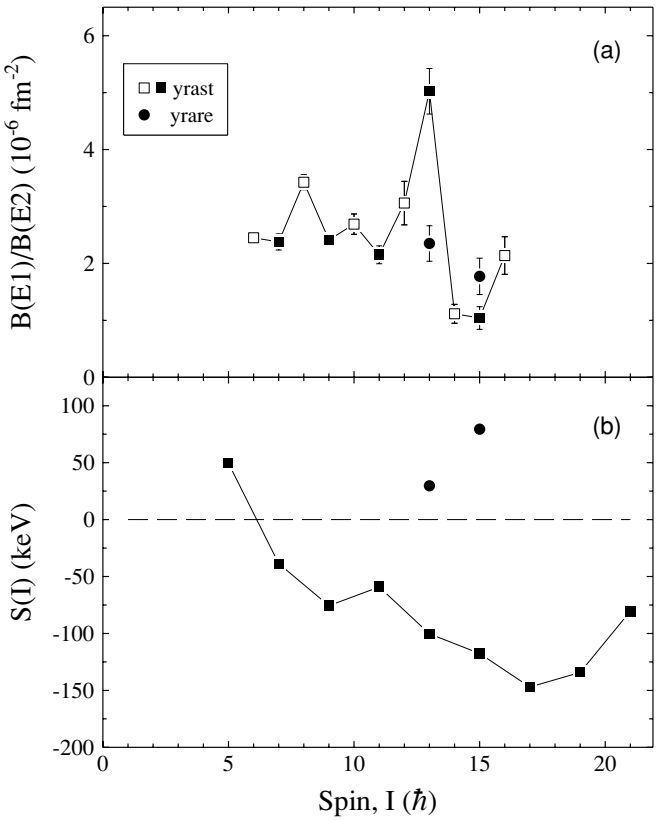

FIG. 5. (a) $B(E1)/B(E2)$ ratios versus initial spin for yrast transitions (squares) and yrare transitions (circles) in ^{220}Th. The yrast states are further distinguished by open and filled squares for even and odd spins, respectively. (b) Parity splitting $S(I)$ for the corresponding states according to expression (1) given in the text.

With the exception of the two data points discussed above, the $B(E1)/B(E2)$ ratios for the yrast states with odd spin (negative parity) lie systematically lower than the ratios for the yrast states with even spin (positive parity). This pattern is in line with the already mentioned staggering of the $E1$ transition energies between consecutive levels of the yrast structure. For a systematic description of this trend, the parity splitting expressed as

$$S(I^-) = E(I^-) - \frac{(I+1)E_{(I-1)^+} + I E_{(I+1)^+}}{2I+1}, \qquad (1)$$

is given in Fig. 5(b). For the odd-spin, yrast states with measured $B(E1)/B(E2)$ ratios, the corresponding $S(I^-)$ values are negative. On the other hand, the two $B(E1)/B(E2)$ ratios for yrare states do not follow the staggering trend and the corresponding $S(I^-)$ values are positive.

V. DISCUSSION

A. Comparison with neighboring nuclei

To quantify the collective behavior of ^{220}Th, absolute $B(E2)$ and $B(E1)$ values for individual states would be needed. Such data were obtained in Ref. [16] for the ^{218}Ra isotone from a lifetime measurement with the recoil-distance Doppler-shift method. The current study does not provide this information. However, $B(E1)/B(E2)$ ratios could be extracted for ^{220}Th, and these quantities can be used for a comparison with neighboring nuclei. There are two possible approaches: either a comparison of the $B(E2)$ values is made by assuming a representative $B(E1)$ value for the measured $B(E1)/B(E2)$ ratios or the procedure is reversed and the $B(E1)$ values are compared. We proceed with the former approach because our discussion focuses mostly on the evolution of rotational-like behavior in this mass region and, thus, requires a systematic comparison of $B(E2)$ values. It would also be difficult to compute an appropriate $B(E2)$ value for ^{220}Th from systematics. Indeed, an analysis using Grodzins's systematics to relate $2 \rightarrow 0$ transition energies with $B(E2)$ values does not appear to be useful in the present case, because the ^{218}Ra lifetime data [16] exhibit a marked deviation from the expected relation between the two quantities. By the same token, the present analysis does not rely on the assumption of a constant (spin-independent) quadrupole deformation for the bands.

The weighted averages of the $B(E2)$ values and the corresponding spin ranges, as obtained from the analysis outlined above, can be found in Table II. The $B(E2)$ and $B(E1)$ data for ^{218}Ra [16] have suitable accuracy for spins $I \leqslant 11$, but the $B(E2)$ value for the $2 \rightarrow 0$ transition is excluded here. The comparison between ^{220}Th and ^{218}Ra is made under the assumption that the $B(E1)$ values in the two isotones are, on average, the same. The average $B(E1)$ probability of Ref. [16] is then used as a normalization factor for ^{220}Th. The size of the $B(E1)/B(E2)$ ratio for the 13^-_1 state in ^{220}Th is likely due to a large change in the $B(E2)$ value and is not considered in the present analysis. For ^{222}Th, the $B(E1)$ values were calculated using the parameter value $D_0 = 0.38$ (7) efm, according to Table IV of Ref. [2]. This set of $B(E1)$ values is then used for the comparison of $B(E2)$ values between ^{220}Th and ^{222}Th [17]. The assumption that ^{220}Th and ^{222}Th have comparable $B(E1)$ values is, perhaps, warranted by the fact that in both nuclei the full simplex-partner band is present up to high spin.

As indicated in Table II, the isotones ^{220}Th and ^{218}Ra have very similar $B(E2)$ values in the spin range under discussion. The comparison between ^{220}Th and ^{222}Th, however, points

TABLE II. Average $B(E2)$ values obtained for ^{220}Th and neighboring ^{218}Ra and ^{222}Th.

Nucleus	Spin Range	$\overline{B(E2)}$ ($10^3 e^2$fm^4)	Comment
^{218}Ra[a]	$4 \leqslant I \leqslant 11$	4.8 (29)	—
^{220}Th[b]	$6 \leqslant I \leqslant 16$[c]	4.6 (16)	$B(E1)$ from ^{218}Ra (constant value)
^{220}Th[b]	$6 \leqslant I \leqslant 16$[c]	6.6 (11)	$B(E1)$ from ^{222}Th (see below)
^{222}Th[d]	$6 \leqslant I \leqslant 15$	9.0 (12)	$B(E1)$ for $D_0 = 0.38(7)$ efm[e]

[a]Reference [16].
[b]This work.
[c]For $I = 13$, only the 13^-_2 state is considered.
[d]References [2,17].
[e]$B(E1; I_i \rightarrow I_f) = \frac{3}{4\pi} D_0^2 \langle I_i 010; I_f 0\rangle^2$, $I_i = I$, $I_f = I - 1$.

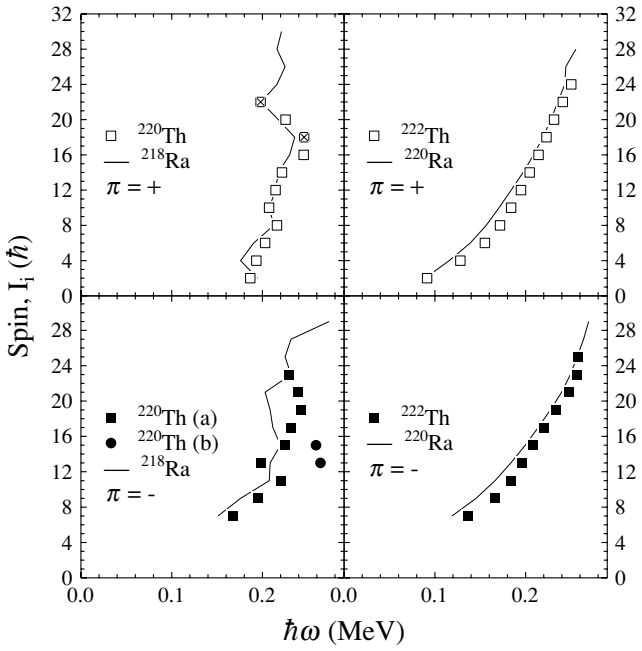

FIG. 6. Spin I_i versus rotational energy $\hbar\omega$ for the yrast $E2$ transitions in ^{220}Th (this work) and ^{218}Ra [5] (left panels) and in ^{222}Th [18] and ^{220}Ra [18] (right panels). The data points marked with crosses are derived from level-energy differences rather than from γ-ray energies.

to larger $B(E2)$ values and, hence, a larger quadrupole deformation for ^{222}Th, provided that the $B(E1)$ values are indeed comparable.

To elaborate further on the different degrees of rotational-like behavior in ^{220}Th and neighboring nuclei, the evolution of the initial spins versus rotational energy is plotted for the yrast structures of a set of nuclei in Fig. 6. The positive-parity and negative-parity $E2$ sequences are shown separately in the panels on the top and the bottom, respectively. Clearly, the yrast structure of ^{220}Th resembles that of its $N = 130$ isotone ^{218}Ra [5], rather than that of ^{222}Th; i.e., ^{220}Th does not exhibit the rotational-like behavior seen in the heavier isotopes. The change occurring between ^{218}Ra and ^{220}Ra is analogous, confirming a structural change with N.

B. Interpretation

For ^{220}Th, the angular velocity ω is approximately constant (Fig. 6), fluctuating around $\omega \sim 0.21$ MeV/$\hbar$, implying that the nucleus does not rotate faster to acquire angular momentum. Multiple band crossings taking place over a broad range of spin values, at the same ω value in two isotones, are considered to be a highly unlikely explanation of the observations and an interpretation in a "traditional" nuclear rotation framework seems difficult. On the other hand, the near-equal spacing of transitions in the yrast structure cannot reflect the presence of spherical vibrational phonons either, as it extends over a large spin range. Instead, the structure of ^{220}Th seems to reflect an intermediate degree of collectivity that is currently a challenge to describe. Several theoretical approaches have been tried for ^{220}Th with varying degrees of success, including the cranked Strutinsky calculations of, e.g., Ref. [19] and the algebraic-model inspired calculations of, e.g., Ref. [20]. Here, we propose a new approach [21] that considers collectivity arising from reflection-asymmetric, constant-velocity nuclear tidal waves, hereby retaining the simplex structure.

The analogous $I(\hbar\omega)$ behavior is seen in band structures built on high-K isomers in ^{182,183}Os [22,23], and it has been interpreted in terms of a rotationally induced triaxial shape. There, the angular momentum is described as developing as a consequence of a simultaneous increase of the triaxiality parameter γ and the angle that measures the tilt of the rotational axis away from the principal axes. The motion corresponds to waves traveling on the triaxial surface with a constant velocity ω. These have been dubbed "nuclear tidal waves" [23]. The emergent level structure consists of two interleaved $\Delta I = 2$ sequences. The presence of these two sequences is a consequence of symmetry breaking due to the tilted axis, whereas the level-energy difference in each sequence $\Delta E \sim \hbar\omega_{\rm vib}(\omega_{\rm vib} = 2 \cdot \omega)$ indicates that the levels are multiphonon like.

We propose that a similar interpretation may apply to the level structures of both ^{220}Th and ^{218}Ra with reflection-asymmetric (octupole) nuclear tidal waves. In this picture, the waves travel with an angular velocity $\omega \sim 0.21$ MeV/$\hbar$. The nuclear shape in the rotating frame of reference is a combination of quadrupole and octupole deformations that both increase with spin, reaching $\beta_2 \sim 0.1$ and $\beta_3 \sim 0.1$ (cf. Fig. 2 of Ref. [5]), respectively. This concept can account not only for the approximately constant level spacing of the "tidal" band but also for the other features of the level schemes discussed hereafter. Detailed calculations to place this interpretation on firmer ground are in progress [21].

Parity-splitting and staggering effects: The occurence of interleaved $\Delta I = 2$ sequences of opposite parity points to the presence of simplex symmetry. However, the very negative $S(I)$ values for the yrast states in ^{220}Th and in ^{218}Ra, and the staggering of the $E1$ transition energies, are consistent with tidal waves rather than with stable deformations. Note that for the heavier Th and Ra nuclei [1,13], $S(I) \gtrsim -60$ keV ($N = 132$) and $S(I) \gtrsim -30$ keV ($N = 134$). In the case of tidal waves, substantial tunneling occurs between the two shapes related to each other by the operation of space inversion which restores the parity. In ^{220}Th, the negative-parity states are yrast for $I \geqslant 7$. As a consequence of the tunneling, the $B(E1)/B(E2)$ ratios exhibit a spin-dependent staggering as do the energies. As the deformed reflection-asymmetric shape stabilizes at larger N, the tunneling is progressively suppressed and $S(I)$ values become much smaller.

Doubling of negative-parity odd-spin states in ^{220}Th: If the nuclear shape has only one reflection plane, perpendicular to the angular momentum, a $\Delta I = 1$ sequence of doublets develops. These doublets have the same parity, which alternates with spin, see Fig. 28 (lower panel) of Ref. [24]. The negative-parity structure (b) in ^{220}Th, which connects by an $E2$ transition to the yrast sequence, could represent the partner of the odd-spin doublets. The even-spin partners associated with the positive-parity, even-spin levels are expected to lie

at higher excitation energy and this could account for their nonobservation in the experiment.

Fluctuations in $I(\hbar\omega)$: The fact that the in-band transition energies are fluctuating around an average value ($E_\gamma \sim 420$ keV) indicates that the realistic nuclear tidal waves have a nonadiabatic nature, in contrast to the model case of surface oscillations. When the spin of the tidal system increases, contributions by the relatively few nucleonic orbitals near the Fermi surface are still noticeable. The fluctuations in the frequency $\hbar\omega$ can be attributed to reorientations of individual nucleonic orbitals. These reorientations can be associated with either a gradual shape change or, perhaps, with a partial alignment of the individual spins with the total angular momentum.

The backbending in the yrast sequence of ^{220}Th at $\hbar\omega = 0.20$ MeV and $I = 13^-$ may be viewed as such an alignment. For $I \geqslant 13$, Fig. 6 (bottom left) shows a gradual difference between ^{220}Th and ^{218}Ra, which may suggest a proton alignment. This effect is perhaps consistent with the predicted rotational alignment of an $i_{13/2}$ proton pair at $\hbar\omega \sim 0.2$ MeV, see Fig. 12 of Ref. [19]. However, in the model using tidal waves, the alignment does not occur as a function of frequency but as a function of spin or shape change. Moreover, it cannot be associated with the breaking of a pure $i_{13/2}$ proton pair if the shape is reflection-asymmetric: there must be an admixture of positive- and negative-parity orbitals.

VI. CONCLUSION

Multiple octupole-type band structures in ^{220}Th have been observed and characterized from evaporation-residue selected γ-ray spectroscopy. The evidence suggests that ^{220}Th has a smaller quadrupole deformation than ^{222}Th. The ^{220}Th nucleus resembles its isotone ^{218}Ra. With four neutrons in excess of the magic number $N = 126$,^{220}Th is located in a transitional region between a noncollective behavior, associated with a spherical nuclear shape, and a collective behavior, with stable and axially symmetric quadrupole and octupole deformations. The common features of ^{220}Th and ^{218}Ra and the staggering of the $B(E1)/B(E2)$ ratios in ^{220}Th may be qualitatively described using a picture where reflection-asymmetric tidal waves travel over the nuclear surface. The shape in the rotating frame is a combination of quadrupole and octupole deformations. The possibility that the shape of ^{220}Th is not axially symmetric, i.e., that it has only one reflection plane, can explain the presence of a second, negative-parity, odd-spin sequence, which is an observation unique to this nucleus. This shape argument is not part of the concept of tidal waves, but is compatible with it. Detailed calculations based on this concept are needed to place the present interpretation on firmer ground; this theoretical effort is in progress. Nuclear tidal waves may well represent a common high-spin phenomenon in transitional regions between different symmetries (spherical and reflection-asymmetrically deformed in the present case); i.e., in regions where these symmetries are weakly broken.

ACKNOWLEDGMENTS

The authors would like to thank J. Elson (W.U.) and J. Rohrer (A.N.L.) for technical support and J.P. Greene (A.N.L.) for the preparation of the target. This work was supported by the U.S. Department of Energy, Office of Nuclear Physics, grants DE-FG02-88ER-40406 and W-31-109-ENG-38.

[1] I. Ahmad and P. A. Butler, Annu. Rev. Nucl. Part. Sci. **43**, 71 (1993); and references therein.
[2] P. A. Butler and W. Nazarewicz, Rev. Mod. Phys. **68**, 349 (1996); and references therein.
[3] I. Wiedenhöver *et al.*, Phys. Rev. Lett. **83**, 2143 (1999).
[4] S. Zhu *et al.*, Phys. Lett. **B618**, 51 (2005).
[5] N. Schulz *et al.*, Phys. Rev. Lett. **63**, 2645 (1989).
[6] O. Häusser, W. Witthuhn, T. K. Alexander, A. B. McDonald, J. C. D. Milton, and A. Olin, Phys. Rev. Lett. **31**, 323 (1973).
[7] W. Bonin, H. Backe, M. Dahlinger, S. Glienke, D. Habs, and E. Hanelt, Z. Phys. A **322**, 59 (1985).
[8] B. Schwartz, Ph.D. thesis, University of Heidelberg (1988).
[9] The ground state of an even-even reflection-asymmetric nucleus has a simplex quantum number $s = +1$. For $s = +1$, the level sequence is 0^+, 1^-, 2^+, 3^-.
[10] The total fusion cross section $\sigma \propto \pi \lambda\!\!\!^{-2} \Sigma_\ell (2\ell + 1)$ for angular momenta $\ell\hbar$.
[11] I. Y. Lee, Nucl. Phys. **A520**, 641c (1990).
[12] W. Reviol, D. G. Sarantites, R. J. Charity, C. J. Chiara, J. Elson, M. Montero, O. L. Pechenaya, S. K. Ryu, and L. G. Sobotka, Nucl. Instrum. Methods A **541**, 478 (2005).
[13] R. B. Firestone and V. S. Shirley, *Table of Isotopes*, 8th ed. (Wiley, New York, 1996), Vol. II.
[14] The method of the isotopic and mass assignments is described in Sec. 3.6 of Ref. [12].
[15] W. Reviol *et al.*, to be published.
[16] M. Gai, J. F. Ennis, D. A. Bromley, H. Emling, F. Azgui, E. Grosse, H. J. Wollersheim, C. Mittag, and F. Riess, Phys. Lett. **B215**, 242 (1988).
[17] D. Ward, G. D. Dracoulis, J. R. Leigh, R. J. Charity, D. J. Hinde, and J. O. Newton, Nucl. Phys. **A406**, 591 (1993).
[18] J. F. Smith *et al.*, Phys. Rev. Lett. **75**, 1050 (1995).
[19] W. Nazarewicz, G. A. Leander, and J. Dudek, Nucl. Phys. **A467**, 437 (1987).
[20] T. Otsuka and M. Sugita, Phys. Lett. **B209**, 140 (1988).
[21] S. G. Frauendorf *et al.*, to be published.
[22] L. K. Pattison *et al.*, Phys. Rev. Lett. **91**, 182501-1 (2003).
[23] D. M. Cullen, R. Glover, L. K. Pattison, P. M. Walker, S. Frauendorf, and D. Almehed, J. Phys. G **31**, S1709 (2005).
[24] S. G. Frauendorf, Rev. Mod. Phys. **73**, 463 (2001).